PAPER • **OPEN ACCESS**

Numerical Modeling and Simulation of a Small-Scale Locomotive Powered by Solid Oxide Fuel Cells

To cite this article: Ahmet Fatih Kaya *et al* 2023 *J. Phys.: Conf. Ser.* **2648** 012055

Numerical Modeling and Simulation of a Small-Scale Locomotive Powered by Solid Oxide Fuel Cells

Ahmet Fatih KAYA[a*], Simone PEDRAZZI[a,b], Alberto MUSCIO[a]

[a]Department of Engineering "Enzo Ferrari" - University of Modena and Reggio Emilia – Via Vivarelli 10/1, 41125, Modena, Italy.

[b]H2MORE - Inter-departmental Center, University of Modena and Reggio Emilia, Via Vivarelli 2 – 41125 Modena, Italy.

[*]Corresponding Author, ahmetfatih.kaya@unimore.it

Abstract. The adverse environmental effects of fossil fuels resulted in a sharp rise in demand for renewable energy sources such as solar, wind, and hydrogen. Environmental pollution might be drastically reduced by using renewable energy sources. Various examples of solid oxide fuel cells being employed in locomotives exist in the literature. This work used numerical techniques to simulate and model a vehicle with eight wheels, considered as a small-scale locomotive powered by solid oxide fuel cells. The feasibility of solid oxide fuel cell-based locomotive was investigated through numerical modeling and simulation. The Matlab-Simulink platform, which includes an electrical system, an energy management system, and vehicle dynamics, was used to run the simulations. Four different locomotive configurations were created, (1) The mass of the locomotive (m) = 65000 kg, operating temperature (T) = 750°C, (2) m = 65000 kg, T = 1000°C, (3) m = 80000 kg, T = 750°C, and (4) m = 80000 kg and T = 1000°C. The performance parameters of the vehicle were recorded after the simulations. These factors are crucial for optimizing the locomotives' design and operation since they provide light on their performance. Future locomotive design and operation may be influenced by the findings of this study, resulting in more environmentally friendly and sustainable transportation networks.

1. Introduction

Since the dawn of humankind, and particularly following the industrial revolution, the amount of energy required has increased rapidly. Initially, the increase in energy demand was met with fossil fuels due to limited technological capabilities. However, the advancement of technology has facilitated the widespread use of renewable energy sources. One of the most important reasons for the rapid spread of the use of renewable energy sources is the emissions of fossil fuels and the global warming caused by these emissions.

The automotive sector has been dependent on the use of internal combustion engine (ICE) technology and fossil fuels quite a bit during the past century. In addition to being inexpensive to manufacture, ICEs are also convenient to manage and fast to refill, but the quantity of CO_2 and other pollutants that today's road automobiles emit reduces air quality [1]. 40% or more of all fossil fuels utilized in the transportation sector are consumed by automobiles [2]. The automobile industry is gradually switching from fossil fuels to renewable energy in order to make the transition to eco-friendly vehicles [1]. One of the biggest obstacles to the global fight against climate change is decarbonizing the transportation sector. Currently, 92% of the energy used in transportation comes from hydrocarbons, which are also responsible for 23%

of all emissions worldwide. Nonetheless, decarbonizing the automotive industry will be an exceedingly difficult task, as mobility represents a critical factor for the energy source, and hydrocarbons are among the most energy-dense materials available in the market [3,4]. Although study into the full effects of locomotive emissions is still ongoing, it is becoming increasingly obvious that the environment and the health of individuals who live close to the centers of operation of the rail lines are under a great deal of stress [5]. Research from Southern California shows the effects of diesel exhaust particle (DEP) emissions on the local population living close to train operations hubs; 29 fatalities, 750 asthma attacks, and up to 6600 missed workdays in a single year, attributed to these DEP emissions from the Ports of Los Angeles and Long Beach [6].

The electrification of transportation systems is crucial for a sustainable future in order to prevent the consequences of the massive consumption of fossil fuels in the future. Parallel initiatives must be made to replace all of these transportation segments' fossil-fuel-based powering systems with more environmentally friendly alternatives in order to minimize emissions. The automotive and transportation industries have seen a number of initiatives to switch from carbon-dense fuels to greener alternatives. Miller et al. designed a system for a large fuel-cell hybrid locomotive. Their proposed system was created to simulate the Vehicle Projects LLC locomotive. The total vehicle layout design schematic was displayed in their study. Additionally, the various subsystems included in the vehicle, such as the power and stack modules, hydrogen storage, and cooling system were designed. The fuel cell stacks used in their investigation had a total output of 300 kW and a direct current (DC) voltage of 624 V. At 350 bar (5100 psi), 70 kg of compressed hydrogen was kept in storage [7]. Hoffrichter et al. assessed the effectiveness of the University of Birmingham-built, the "Hydrogen Pioneer" is a prototype locomotive that operates on hydrogen power. The locomotive uses a proton exchange membrane fuel cell (PEMFC) to generate energy for the on-board lead-acid batteries or traction motors using hydrogen gas. The effectiveness of the car, the power source, and the hybrid system's operation were all calculated. The hybrid locomotive has a maximum speed of 20 km/h and a mass of 270 kg without a hydrogen tank. Their fuel cell can produce a maximum of 1.1 kW of power. They employed the 2.2 kW permanent magnet traction motor LEM-130/95. A 12V 90 Ah EXV90 Enduroline calcium leisure battery pack was also utilized [8]. An experimental prototype of a PEMFC shunting locomotive that will have less of an impact on the environment has been constructed through innovation of the power system utilizing PEMFC by Peng et al. Experimental research is done to determine how well the combined locomotive and fuel cell power plant function. It is China’s first locomotive to employ a PEMFC power plant. The mass of the train is approximately 45 tons. In the model, the continuous speed is 21 km/h, the maximum operating speed is 65 km/h and the tractive motor power is 240 kW [9]. Guo et al. described and designed a fuel cell hybrid switcher locomotive's power system. With the Matlab/Simulink simulation tool, the solid oxide fuel cell (SOFC) model was created. During their research, they evaluated various types of fuel cells that could be used in locomotives and developed models for fuel cell and additional storage systems. They observed the output voltages of different power sources and the state of charge of the battery pack [10]. Torreglosa et al. used fuzzy logic and cascade-based control in a fuel-cell hybrid tramway model. They presented a concept for a hybrid system consisting of a fuel cell and battery to power the Metro-Centro tramway with a capacity of 400 kW. Models for Ni-MH batteries and PEMFC were created. They also observed the tramway speed, traction power, fuel cell and dc bus voltage, fuel cell power, battery power and battery SOC [11]. The fuel cell-battery-supercapacitor hybrid tramway's energy management system has been developed by Li et al. They utilized the real driving cycle for an LF-LRV tramway in Turkey. Their model consists of a 150 kW PEMFC, 50 Ah and 518V Li-ion battery pack (2 parallel) and 30 Farad 528 V (11 series 2 parallel) supercapacitor. They observed the output power, voltage, current and efficiency of the PEMFC system, battery bank and supercapacitor bank [12]. Miller et al. made a cost analysis for a 1.2 MW road switcher locomotive for different hybrid configurations. In their study, they calculated the total cost of the system by changing the capacity of batteries and the rated power of the fuel cell system [13]. Schroeder and Majumdar examined the use of SOFC’s with on-board biodiesel gasification to generate electricity for long-haul or road train locomotives. To determine the feasibility of this power system relative to the typical ICE engine/generator power systems, the researchers evaluated different equipment sizes, efficiencies, and

life cycle costs. According to the investigation, it is theoretically possible to operate locomotives with SOFC's that use on-board gasified biodiesel. It is more challenging to justify economic decisions, nevertheless [14]. Haseli et al. conducted a comparison of four different propulsion technologies, namely conventional diesel ICE, electrified train, hydrogen ICE, and PEMFC train, regarding their CO_2 emissions. The results of their study indicate that the most ecologically advantageous option is a PEMFC powertrain fueled by hydrogen generated through a combination of wind energy and a copper-chlorine plant, with CO_2 emissions amounting to approximately 9% of those produced by a typical diesel train [15]. Martinez et al. performed a feasibility analysis of a hybrid locomotive power plant that combines a SOFC and a gas turbine. They conducted preliminary investigations on the system's capability to operate using conventional diesel fuel, natural gas, and hydrogen. Based on their findings, they determined that the system could function efficiently and with manageable dynamic response on all three types of fuel [16].

Motapon et al. developed a Matlab-Simulink model for a vehicle that shares identical characteristics to the Honda FCX-Clarity. Their model is general and capable of simulating the behavior of the majority of hydrogen and air-fueled fuel cells. In their study, they calculated the fuel consumption, maximum speed, acceleration and other performance parameters of the PEMFC vehicle. Their model consists of the battery pack, PEMFC and electric motor [17]. The model can be found in the MATLAB File Exchange window [18]. In the present study, a similar system was designed for a small-scale locomotive using a SOFC. Performance parameters, such as the acceleration, rotor speed, fuel consumption and battery SOC were also calculated with the created model.

2. Material and Method

Fuel cell technology represents a novel and highly promising approach towards replacing combustion engines in vehicles due to its ability to convert the chemical energy of fuel into electrical energy. This innovative technology offers significant potential for improving the efficiency and reducing the harmful emissions associated with traditional combustion engines. They are often considered a new era of technical advancement due to their outstanding efficiency and low emissions [19]. Figure 1 shows the schematic view of the structure of a fuel cell [20]. A common type of fuel cell includes two electrodes, the anode and cathode, where a reaction occurs. The anode and cathode also serve as the pathway for the flow of electrical current. Many fuel cells do not utilize pure hydrogen as a fuel source but instead use a reformer to convert the fuel into hydrogen. Methane, ammonia, gasoline, natural gas, ethanol and some other materials can be used as a fuel for a fuel cell.

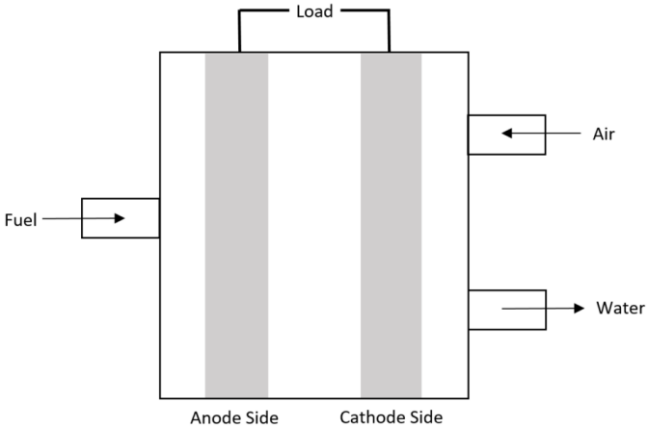

Figure 1. A schematic representation of a fuel cell [20]

Fuel cells are categorized based on the type of electrolyte material they use. PEMFCs, SOFCs, phosphoric acid fuel cells (PAFCs), alkaline fuel cells (AFCs), and molten carbonate fuel cells (MCFCs)

are some examples of fuel cell types. Table 1, which summarizes the various fuel cell types and their characteristics, is presented in references [1,21].

Table 1. Fuel cell types

Parameters	Fuel Cell Types				
	PEMFC	**SOFC**	**AFC**	**PAFC**	**MCFC**
Electrolyte	Polymeric membrane	Ceramics	Potassium hydroxide	Phosphoric acid	Molten carbonate
Working Temperature	Between -40°C and 120°C	500-1000°C	50-200°C	150-220°C	600-700°C
Efficiency	As high as 65-72%.	As high as 65%.	As high as 70%	As high as 45%.	As high as 60%.
Fuel	Hydrogen, reformed Hydrogen	Hydrogen, biogas, or methane	Hydrogen or cracked ammonia	Hydrogen, reformed Hydrogen	Hydrogen, biogas, or methane

The ability to process a wide range of fuels is one advantage of SOFCs with a high-temperature range and effective oxidizing ion transfer [22]. As mentioned in the introduction section, SOFCs can be used for locomotives or other types of railway vehicles. So, in this study, a vehicle (which can be considered as a small-scale locomotive with eight wheels) with a mass of 65000 kg and 80000 kg were designed. For two different operating temperatures (750°C and 1000°C), performance parameters were estimated. The fuel cell stack was created from the MATLAB Library Browser (Simscape / Electrical / Specialized Power Systems / Sources). In this model, users can define the nominal operating point and the maximum operating point of the fuel cell. In this way, it is possible to create a polarization (I-V) curve. To run the model, stack efficiency, operating temperature and pressure values of fuel and air should also be provided [17].

One can derive the equation for the stack output voltage V_{fc} of a fuel cell by utilizing Nernst's equation and simultaneously accounting for voltage losses, including ohmic, activation, and concentration losses [23].

$$V_{fc} = E_N - V_{act} - V_{con} - V_{ohm} \tag{1}$$

In this equation, E_N is the Nernst voltage (V), V_{act} is the activation voltage loss (V), V_{con} is the concentration (mass transportation) losses (V) and V_{ohm} is the ohmic losses (V). V_{act}, V_{con} and V_{ohm} can be calculated as [23,24];

$$V_{act} = -Aln(i) \tag{2}$$

$$V_{con} = m * e^{ni} \tag{3}$$

$$V_{ohm} = r * I_{fc} \tag{4}$$

In these formulas, A depicts the Tafel slope (V, constant for SOFC), i is the current density (A/m^2), m and n are the constant from the experiments, r is the internal resistance (ohm) and I_{fc} is the fuel cell current (A).

E_N for the SOFCs can be calculated with the following equation [17];

$$E_N = 1.229 + (T - 298) * \frac{-44.43}{2F} + \frac{RT}{2F} \ln\left(\frac{P_{H_2} {P_{O_2}}^{0.5}}{P_{H_2O}}\right) \tag{5}$$

Here, T is the stack temperature (K), R is the gas constant (8.3145 J/(mol K), F is the Faraday constant (96485 A s/mol), P_{H_2}, P_{O_2} and P_{H_2O} show the partial pressure (atm) of hydrogen, oxygen and water vapor, respectively and calculated as [17];

$$P_{H_2} = \left(1 - Uf_{H_2}\right)x\%P_f \tag{6}$$

$$P_{O_2} = \left(1 - Uf_{O_2}\right)y\%P_a \tag{7}$$

$$P_{H_2O} = \left(w + 2y\%Uf_{O_2}\right)P_a \tag{8}$$

$$Uf_{H_2} = \frac{60000RTI_{fc}}{2FP_fV_fx\%} \tag{9}$$

$$Uf_{O_2} = \frac{60000RTI_{fc}}{4FP_aV_ay\%} \tag{10}$$

In these equations, Uf is the rate of utilizations, x and y show the hydrogen percentage in the fuel and oxygen percentage in the air, respectively. P_f is the absolute pressure of the fuel (atm), P_a is the absolute pressure of the air (atm), V_f is the fuel flow rate (l/min), V_a is the airflow rate (l/min) and w is the water vapor in the air (%) [17]. The value of 60000 is derived from converting the flow rate used in the model from liters per minute to cubic meters per second, where one liter per minute is equivalent to 1/60000 cubic meters per second.

For the experimental validation of a SOFC stack, the SOFC was created, the operating points were defined and I-V and current-power (I-P) curves were created for a SOFC. Figure 2 compares the experimental [25] and the numerical I-V and I-P curves. As seen in Figure 2, the numerical and experimental results are similar, especially when the current is higher than 300 A. In the present model, the vehicle is assumed to have an 840 kW SOFC stack, so the total number of fuel cell stacks is assumed to be six since the stack power validated is approximately 140 kW.

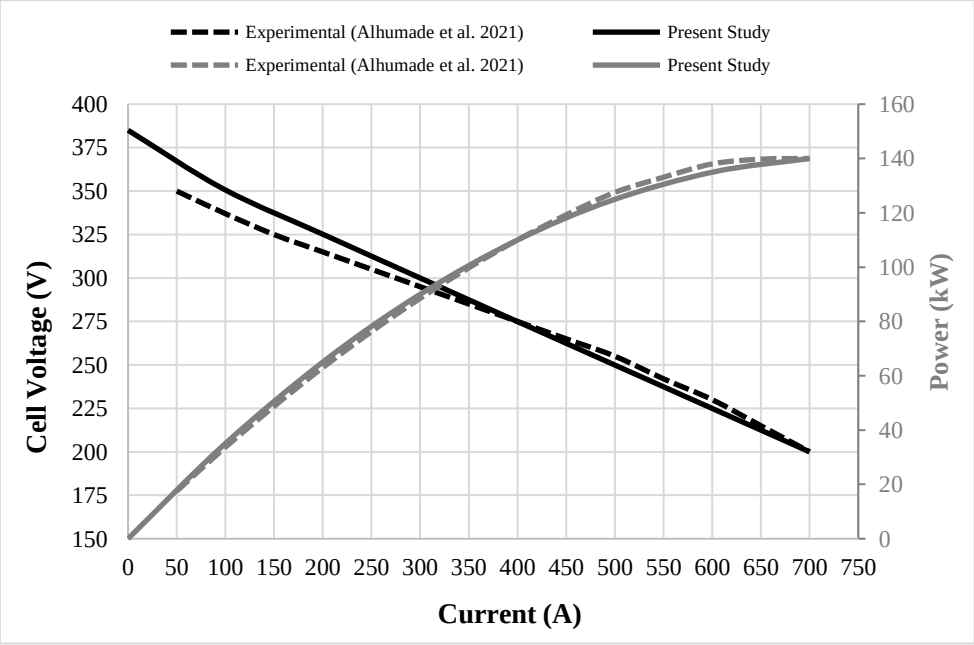

Figure 2. Comparison of experimental [25] and numerical polarization curves

Battery packs are an essential component of many modern technologies, including electric vehicles, renewable energy systems, and industrial equipment. When designing or analyzing a battery pack, it is important to understand its key characteristics, such as nominal voltage, rated capacity, and state of charge (SOC). In the present study, the total capacity of 72 kWh battery pack is considered. Additionally, the model assumes an initial SOC of 50%, meaning that the available energy at the beginning of the locomotive operation is 36 kWh. However, it is important to note that this model neglects temperature effects, which can significantly impact the performance and lifespan of the battery pack. Temperature can affect the battery's internal resistance, charge acceptance, and self-discharge rate, among other factors. Therefore, any battery modeling or analysis should carefully consider temperature effects to obtain accurate results. The battery is utilized in an additional capacity to support the fuel cell stack, and the energy management subsystem effectively allocates power among these sources. A permanent magnet synchronous motor with a maximum 800 kW rated power was designed for the electric motor. The torque–speed characteristic of the selected electric motor was selected the same as in Motapon et al.'s study [17].

$$P_{motor} = T_{motor} * \omega_{rad/sec} \tag{11}$$

$$\omega_{rad/sec} = (\omega_{rpm} * \pi)/30 \tag{12}$$

Here, P_{motor} is the rated power of the electric motor (W), T_{motor} is the torque (N.m) and ω is the rotational speed, radian/second or round per minute (rpm). Vehicle speed (km/h) can be calculated as;

$$Vehicle\ Speed\ (km/h) = \frac{3{,}6 * \omega_{rpm} * \pi * r_w}{30 * i_g * i_f} \tag{13}$$

In this equation, r_w is the wheel radius (m), i_g is the gearbox gear ratio and i_f is the final drive ratio.

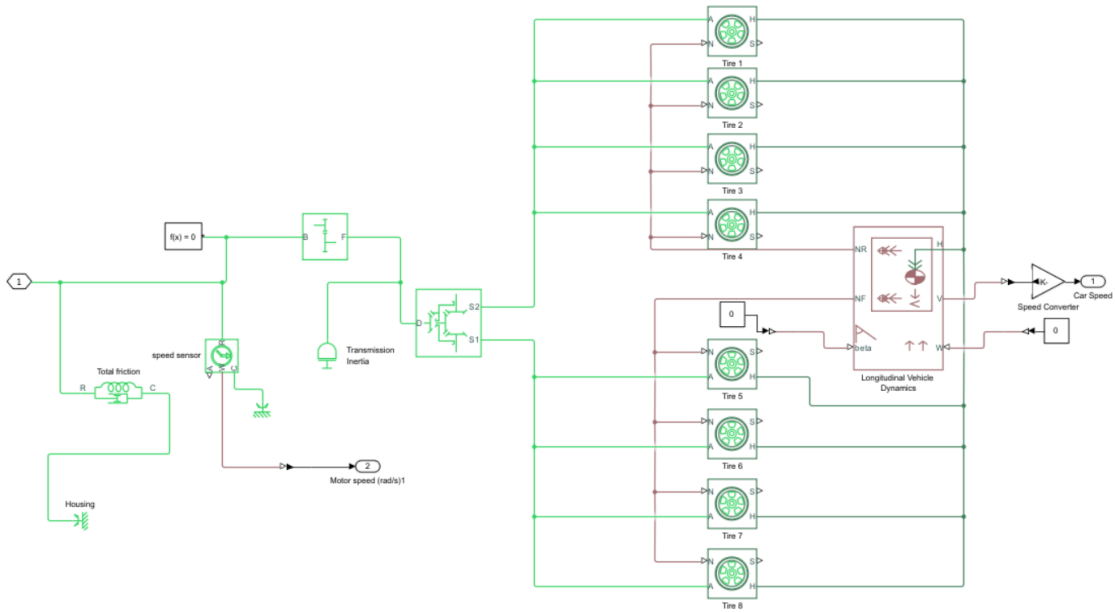

Figure 3. The vehicle dynamics setup

Figure 3 shows the vehicle dynamics setup of the modelled locomotives. Angular velocity or angle is measured by a speed sensor in a mechanical rotational network. A simple gear depicts a gear or gear box with a fixed-ratio. Longitudinal vehicle dynamics block represents a vehicle body with two axles moving longitudinally. The block takes into account weight distribution between axles caused by acceleration and road profile, as well as body mass, aerodynamic drag, road inclination, and other factors

[26]. The gear ratio was selected as 4.04 and the wheel radius was chosen as 0.46 meter. These values were defined close to the real data of an electric locomotive [27].

3. Results

In the present study, four different configurations were created; (1) The mass of the locomotive (m) = 65000 kg, T = 750°C, (2) m = 65000 kg, T = 1000°C, (3) m = 80000 kg, T = 750°C, and (4) m = 80000 kg and T = 1000°C. The current simulations were conducted under the constant full acceleration condition. This decision was made to simplify the simulation and focus on the effects of vehicle mass and SOFC operating temperature. Specifically, the accelerator was fully engaged for the entirety of the 100-second simulation period, and the locomotive was assumed to be operating on a level track with negligible wind resistance. These assumptions allowed us to isolate the effects of vehicle mass and SOFC operating temperature on the locomotive's performance.

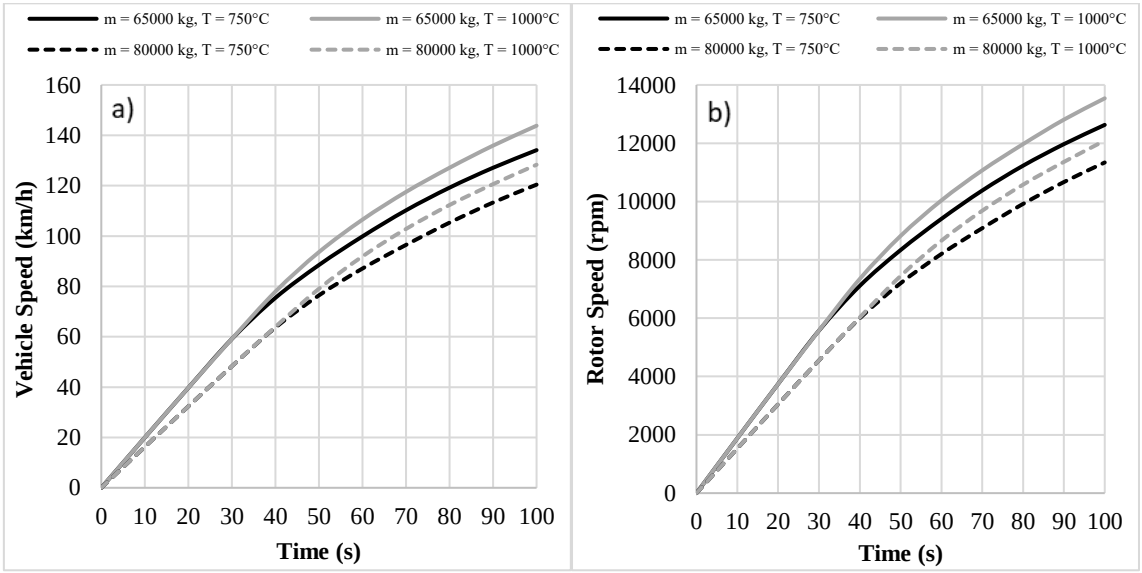

Figure 4. a) Vehicle speed b) rotor speed versus Time

Figure 4 shows the vehicle speed (km/h) and the rotational speed of the electric motor (rpm). The rotor speed and vehicle speed are directly inversely correlated with electric vehicles. The rotor, which powers the car's wheels, is what propels the vehicle, hence the motor rotor's speed directly affects the vehicle's speed. Due to the law of inertia, an 80000 kg vehicle will typically accelerate more slowly than a 65000 kg vehicle. The propensity of an object to resist modifications to its motion is known as inertia, and it is dependent on the object's mass. An object's inertia increases with mass, which means it takes more force to change its motion. Each vehicle's acceleration is likely controlled by the SOFC's power output, which is affected by the vehicle's mass and its temperature. Since the vehicle mass is the lowest (65000 kg) and the SOFC temperature is the highest (1000°C), the SOFC's power output is increased the most in this configuration, and the vehicle may accelerate swiftly with that power. To obtain a more accurate representation of the train's performance, it's recommended that more precise values for all parameters such as drag coefficient, centre of mass of the train etc. must be determined through further analysis or experimentation. Without such information, the interpretation of the simulation results should be approached with caution, as the actual performance of the SOFC train could differ from what was simulated.

Figure 5 shows the electromagnetic torque values obtained from the electric motor. In general, it is true that as rotor speed rises, electromagnetic torque generated by an electric motor decreases. This is because the motor's back electromotive force (EMF), which opposes the applied voltage and lowers the net voltage across the motor windings, is the cause of the issue. The back EMF grows as the rotor speed

rises, lowering the net voltage and, consequently, the electromagnetic torque. Since the rotor speed increases slower for an 80000 kg vehicle, it is possible to say the electromagnetic torque values also decrease more slowly. It was stated that the electromagnetic torque usually declines with the rotor speed increase. However, At time = 50s, the electromagnetic torque was observed as 689,4 Nm and rotor speed was calculated as 8337 rpm (see Figure 4b) for a 65000 kg vehicle and 750°C stack. At the same time, the electromagnetic torque value was calculated as 815,2 Nm and the rotor speed was equal to 8822 rpm for a 65000 kg vehicle and 1000°C stack. The reason behind this is that at higher temperatures, the SOFC stack may be able to produce more electrical power, which could result in higher electromagnetic torque at a given rotor speed.

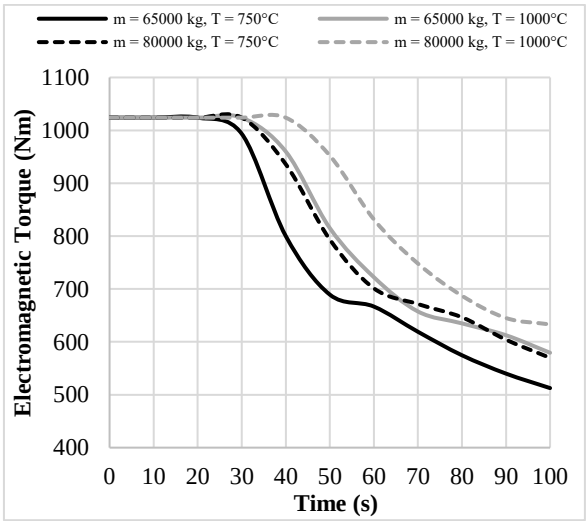

Figure 5. Electromagnetic torque versus time

Figure 6 shows SOFC stack and the motor power changing with time. The slopes are not the same, but they are similar. The maximum stack power was calculated as 804,5 kW for the vehicle with m = 65000 kg and T = 1000°C. Fuel cell devices often generate more power at higher temperatures. This is due to the temperature dependence of the chemical reactions that occur within the fuel cell, which can lead to faster and more efficient reactions at higher temperatures.

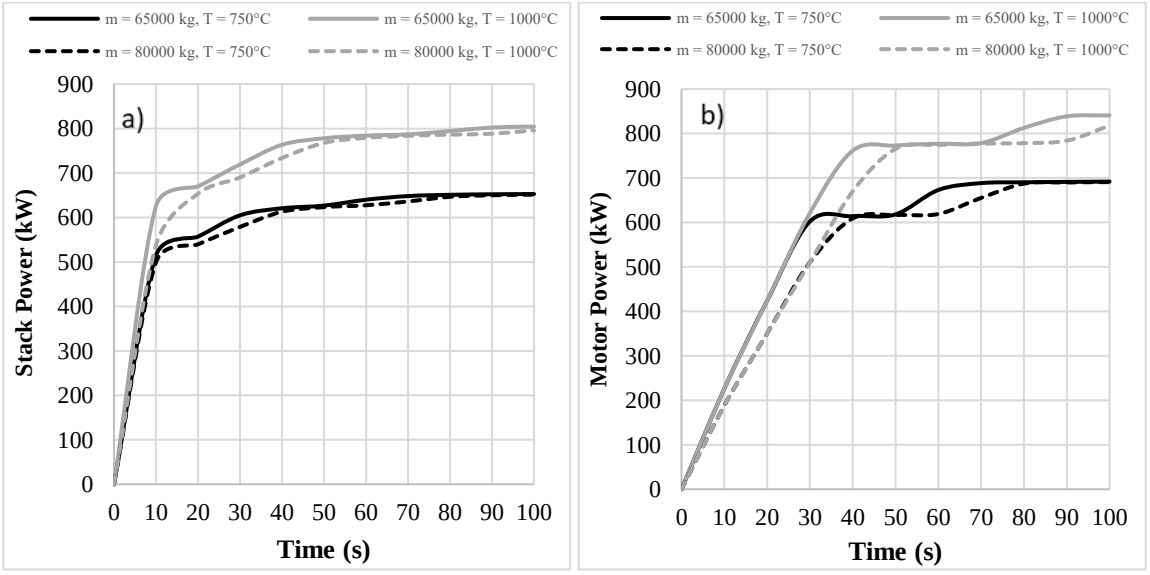

Figure 6. a) Stack power b) motor power versus time

However, operating a SOFC at higher temperatures can also have drawbacks like decreased durability and increased fuel cell component degradation. It is worth noting that the motor's power output is also dependent on the specific design of the motor, the voltage and current supplied by the SOFC system, and other factors. The maximum motor power was observed as 840,7 kW for the vehicle with m = 65000 kg and T = 1000°C. The needed energy (difference between the motor power and the stack power) was supplied from the battery pack.

Figure 7 shows the hydrogen consumption of SOFC stacks for different vehicle configurations. The vehicle's weight, the road's gradient, the aerodynamic drag, the rolling resistance of the tires, the particular design of the fuel cell stack, and the operating circumstances all impact how much hydrogen a SOFC vehicle uses. Due to its greater weight and higher SOFC operating temperature, the vehicle with m = 80000 kg, T = 1000°C consumes the most fuel. Because of the heavier combined weight, the SOFC system must produce more power to counteract the drag, which increases fuel consumption. Furthermore, while the SOFC system's higher operating temperature in the same vehicle may increase system efficiency, it can also result in increased degradation and reduced durability of the fuel cell components. The simulation results indicate that the vehicle, weighing 65000 kg and an operating temperature of 750°C, had the most minor fuel consumption compared to the other vehicles in the study. The lower fuel consumption of this vehicle is likely due to its lighter weight and lower operating temperature of the SOFC system.

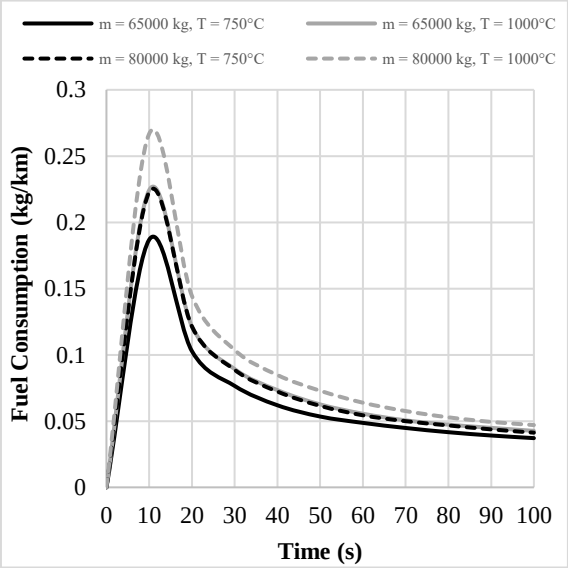

Figure 7. Hydrogen consumption versus time

Figure 8 shows the battery SOC percentage changing with time. The simulation results presented in this study indicate that the difference between the SOFC stack power and the motor power is higher at the beginning of the simulation for all vehicle models. This means that the SOFC system initially produces more power than the motor consumes, resulting in excess power that can be stored in the battery. As a result, the battery SOC increases faster at the beginning of the simulation, which can have implications for the overall performance and efficiency of the vehicle. The faster increase in battery SOC at the beginning of the simulation may be due to several factors, including the initial power demand of the motor, the specific design of the SOFC stack and electric motor, and the vehicle's operating conditions. However, as the simulation progresses and the power demand of the motor increases, the difference between the SOFC stack power and the motor power decreases, and the rate of increase in battery SOC also slows down. The vehicle weighing 80000 kg and an operating temperature of 1000°C exhibits the highest difference between the SOFC stack power and the motor power at the beginning of the simulation. As a result, the battery SOC increases faster for this vehicle model than the other models.

At some point, for all vehicle configurations, battery SOC starts to decline. This is due the motor power is higher than the stack power (see Fig. 6) and battery pack is used to compensate this power difference.

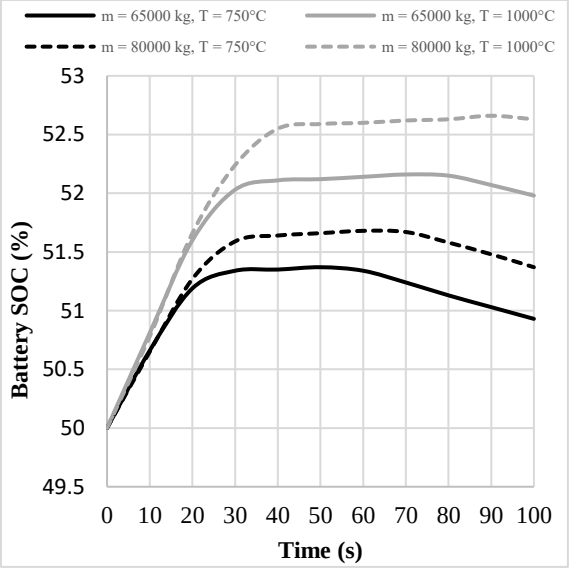

Figure 8. Battery SOC versus time

4. Conclusion

Based on the simulation results presented in this study, the vehicle's weight and the operating temperature of the SOFC system are critical factors that affect the performance and fuel consumption of SOFC vehicles. The simulations were conducted for four different vehicle configurations, and the performance graphs of the vehicle, fuel cell stack, and electric engine were created. The results showed that the rotor and vehicle speed are directly inversely correlated in electric vehicles, and the vehicle's mass affects the acceleration due to the law of inertia. The electromagnetic torque values obtained from the electric motor were found to decline with increasing rotor speed. The hydrogen consumption of the SOFC stacks varied for different vehicle configurations. The vehicle with the lowest fuel consumption weighed 65000 kg and had an operating temperature of 750°C. The simulation results also show that for all vehicle models, the SOFC stack power and the motor power difference are more significant at the start of the simulation, leading to faster increases in battery SOC. At some point, battery SOC starts to decline, because of the stack cannot meet the power demand of vehicle.

While the created performance graphs provides a useful visualization of the SOFC locomotive, it should be noted that the vehicle dynamics can have a significant impact on its overall performance. Factors such as rolling resistance, aerodynamic drag and other vehicle-specific parameters can affect the locomotive’s acceleration, top speed, and overall efficiency. Therefore, in order to fully understand the capabilities of the SOFC locomotive, more detailed analyses of these parameters should be performed. By taking into account these additional variables, we can gain a more accurate understanding of the locomotive’s true performance potential, and identify areas where optimization can be achieved.

Overall, these findings suggest that optimizing the design and operating conditions of a SOFC system for a given application and power demand is critical in achieving lower fuel consumption and improved efficiency. The vehicle's weight and the operating temperature of the SOFC system are two key factors to consider when designing and optimizing SOFC vehicles for sustainable transportation applications. By carefully balancing efficiency and durability, it may be possible to develop SOFC vehicles that offer a practical and sustainable alternative to conventional ICE vehicles.

A promising direction for future research involves the integration of real-world drive cycles into the simulation model. As it stands, the model operates under the assumption of constant full acceleration, a

simplification of actual locomotive operation. The introduction of real-world drive cycles could allow future simulations to capture the varying speed profiles and operating conditions typical of real locomotive operation, thus offering a more accurate performance assessment. In addition, the model could be extended to include and compare various types of locomotives, encompassing not only SOFC-powered locomotives but also battery electric, diesel, and gas turbine-SOFC hybrid locomotives. This expansion would enable a comprehensive comparison of these different propulsion technologies in their performance, efficiency, and environmental impact. With such a comparison, CO2 emissions could be estimated, shedding light on the environmental benefits or drawbacks of each technology. Future research could also involve refining the vehicle model used in the simulations. For instance, a more detailed locomotive model, capable of calculating the drag coefficient, could render the simulation more realistic. The inclusion of other factors, such as vehicle geometry, wind resistance, and track gradient, could further improve the realism and accuracy of the simulation.

5. References

[1] Aminudin M A, Kamarudin S K, Lim B H, Majilan E H, Masdar M S and Shaari N 2023 An overview: Current progress on hydrogen fuel cell vehicles *Int. J. Hydrogen Energy* **48** 4371–88

[2] Berggren C and Magnusson T 2012 Reducing automotive emissions-The potentials of combustion engine technologies and the power of policy *Energy Policy* **41** 636–43

[3] Boldrin P and Brandon N P 2019 Progress and outlook for solid oxide fuel cells for transportation applications *Nat. Catal.* **2** 571–7

[4] Edenhofer O et al. 2014 *IPCC Climate Change 2014: Mitigation of Climate Change*

[5] Martinez A S, Brouwer J and Samuelsen G S 2012 Feasibility study for SOFC-GT hybrid locomotive power part II. System packaging and operating route simulation *J. Power Sources* **213** 358–74

[6] California Air Resources Board 2006 *Diesel Particulate Matter Exposure Assessment Study for the Ports of Los Angeles and Long Beach* (Sacramento, CA)

[7] Miller A R, Hess K S, Barnes D L and Erickson T L 2007 System design of a large fuel cell hybrid locomotive *J. Power Sources* **173** 935–42

[8] Hoffrichter A, Fisher P, Tutcher J, Hillmansen S and Roberts C 2014 Performance evaluation of the hydrogen-powered prototype locomotive “Hydrogen Pioneer” *J. Power Sources* **250** 120–7

[9] Peng F, Chen W, Liu Z, Li Q and Dai C 2014 System integration of China’s first proton exchange membrane fuel cell locomotive *Int. J. Hydrogen Energy* **39** 13886–93

[10] Guo L, Yedavalli K and Zinger D 2011 Design and modeling of power system for a fuel cell hybrid switcher locomotive *Energy Convers. Manag.* **52** 1406–13

[11] Torreglosa J P, Jurado F, Garca P and Fernndez L M 2011 Application of cascade and fuzzy logic based control in a model of a fuel-cell hybrid tramway *Eng. Appl. Artif. Intell.* **24** 1–11

[12] Li Q, Chen W, Liu Z, Li M and Ma L 2015 Development of energy management system based on a power sharing strategy for a fuel cell-battery-supercapacitor hybrid tramway *J. Power Sources* **279** 267–80

[13] Miller A R, Peters J, Smith B E and Velev O A 2006 Analysis of fuel cell hybrid locomotives *J. Power Sources* **157** 855–61

[14] Schroeder D J and Majumdar P 2010 Feasibility analysis for solid oxide fuel cells as a power source for railroad road locomotives *Int. J. Hydrogen Energy* **35** 11308–14

[15] Haseli Y, Naterer G F and Dincer I 2008 Comparative assessment of greenhouse gas

mitigation of hydrogen passenger trains *Int. J. Hydrogen Energy* **33** 1788–96

[16] Martinez A S, Brouwer J and Samuelsen G S 2012 Feasibility study for SOFC-GT hybrid locomotive power: Part I. Development of a dynamic 3.5 MW SOFC-GT FORTRAN model *J. Power Sources* **213** 203–17

[17] Motapon S N, Tremblay O and Dessaint L A 2012 Development of a generic fuel cell model: Application to a fuel cell vehicle simulation *Int. J. Power Electron.* **4** 505–22

[18] Pierre Mercier 2023 Fuel Cell Vehicle (FCV) Power Train

[19] Wang Y, Seo B, Wang B, Zamel N, Jiao K and Adroher X C 2020 Fundamentals, materials, and machine learning of polymer electrolyte membrane fuel cell technology *Energy AI* **1** 100014

[20] Miao Z, M.A. C, Klein R L and Fan L 2004 Study of A Fuel Cell Power Plant in Power Distribution System – Part I: Dynamic Model *2004 IEEE Power Eng. Soc. Gen. Meet.* **2** 2220–5

[21] Yu Y, Tu Z, Zhang H, Zhan Z and Pan M 2011 Comparison of degradation behaviors for open-ended and closed proton exchange membrane fuel cells during startup and shutdown cycles *J. Power Sources* **196** 5077–83

[22] Manoharan Y, Hosseini S E, Butler B and Alzhahrani H 2019 Hydrogen Fuel Cell Vehicles; Current Status and Future Prospect *Appl. Sci.* **9**

[23] Roy S 2016 Implementation of Model to Analyse the Performance of Microturbine as in Microgrid Comparison with Fuel Cell *Int. J. Energy Optim. Eng.* **5** 19–42

[24] Boccaletti C, Fabbri G, Riot O and Santini E 2007 Modeling and simulation of hybrid SOFC-GT systems for distributed generation *Renew. Energy Power Qual. J.* **1** 243–50

[25] Alhumade H, Fathy A, Al-Zahrani A, Rawa M J and Rezk H 2021 Optimal parameter estimation methodology of solid oxide fuel cell using modern optimization *Mathematics* **9** 1–19

[26] Https://www.mathworks.com/help/sdl/ref/vehiclebody.html. MATLAB Documentation.

[27] Mcsparran L W 1974 E60c Electric Locomotives for the Black Mesa and Lake Powell Railroad *IEEE Trans. Ind. Appl.* **IA-10** 385–90